Journal of Biological Research 1 (2), 2026: pp. 1-8.

Original article

IRSTI: 34.19.23 **https://doi.org/10.70264/jbr.v1.2.2026.1**

MIRNA-4739 TARGETS URM1 TO INHIBIT JNK SIGNALING AND PROMOTE APOPTOSIS IN GASTRIC CANCER

Yaochu Zheng*, Yanyan Xiong, Zhitai Zhu

Department of Gastroenterology, Yingtan People's Hospital,Yingtan 335000, Jiangxi, China

*Corresponding author: Zheng Y., ytsrmyyzyc@163.com

ABSTRACT

This study aimed to investigate the expression and clinical significance of miR-4739 and URM1 in gastric cancer (GC), clarifies their roles and molecular mechanisms in regulating GC cell proliferation, migration, invasion, apoptosis, and oxidative stress, and identifies potential biomarkers and therapeutic targets for GC. Fifty pairs of GC tissue and adjacent normal tissue samples were collected. qPCR was used to detect the expression of miR-4739 and URM1, and their correlations with clinicopathological parameters and TNM stage were analyzed. A dual-luciferase reporter assay verified the direct relationship between miR-4739 and URM1. The human GC cell line NCI-N87 was transfected with the miR-4739 mimic, pcDNA3-URM1, or negative control. CCK-8 and transwell assays were used to detect cell proliferation, migration, and invasion. Western blotting was used to detect URM1, p-JNK and Caspase-3. Co-immunoprecipitation (Co-IP) confirmed the interaction between URM1 and JNK. The levels of intracellular reactive oxygen species (ROS) and protein disulfide bonds were measured to evaluate oxidative stress. The JNK inhibitor SP600125 was used for rescue experiments. miR-4739 was significantly down regulated, and URM1 was upregulated in GC tissues, and its expression levels were closely correlated with TNM stage (T3/T4) and tumor invasion depth ($p<0.01$). miR-4739 directly targets and negatively regulates URM1. Over expression of miR-4739 inhibited the proliferation, migration, and invasion of NCI-N87 cells; promoted apoptosis; reduced the expression of URM1 and p-JNK, increased Caspase-3 level, and alleviated oxidative stress. Over expression of URM1 reversed the effects of miR-4739. Co-immunoprecipitation confirmed a direct interaction between URM1 and JNK. Inhibition of JNK signaling blocks URM1-mediated oxidative stress and malignant biological behavior. miR-4739 is expressed at low levels in GC and serves as a tumor suppressor. By targeting URM1, miR-4739 inhibits JNK signaling pathway activation, reduces oxidative stress, promotes apoptosis, and ultimately suppresses the malignant progression of GC. Thus, the miR-4739/URM1/JNK axis may be a potential diagnostic biomarker and therapeutic target for GC.

Keywords: gastric cancer; miRNA-4739; URM1; apoptosis; JNK signaling; disulfide bonds.

Received: April 29, 2026 / *Accepted*: June 06, 2026 / *Published*: June 27, 2026

Citation: Zheng Y., Xiong Y., Zhu Zh. miRNA-4739 targets URM1 to inhibit JNK signaling and promote apoptosis in gastric cancer. Journal of Biological Research, 1(2), 1-8. https://doi.org/10.70264/jbr.v1.2.2026.1.

1. INTRODUCTION

In recent years, the incidence of gastric cancer has gradually declined owing to improved hygiene and dietary habits. However, it remains the fifth most common cancer globally and the third leading cause of cancer mortality [1]. The high mortality rate is primarily due to inadequate early diagnosis and ineffective treatments [2]. Currently, surgical treatment, immunotherapy, and targeted therapy are the primary strategies for gastric cancer management; however, survival rates and prognoses remain poor in many patients. Moreover, acquired or intrinsic drug resistance in gastric cancer cells further deteriorates the prognosis of chemotherapy recipients [3].

Recently, microRNAs (miRNAs) have emerged as pivotal tools in cancer and other diseases. miRNAs are stable in body fluids, shielded by exosomes, and thus, protected from endogenous RNA degradation enzymes [4]. miRNAs are non-coding single-stranded small RNA of 19-25 nucleotides, primarily regulate cell proliferation, invasion, and migration by suppressing or enhancing the expression of specific genes. Recent studies [5] have indicated that miR-4739 functions as a suppressor in prostate cancer, reducing its expression and stimulating the proliferation and migration of prostate cancer cells. Similarly, gastric cancer research has indicated that TYMSOS triggers the progression, migration, and invasion of gastric cancer cells by regulating ZNF703 and sequestering miR-4739 [6]. However, the role and mechanism of miR-4739 in gastric cancer cell proliferation, migration, invasion, and apoptosis remain unclear.

In human eukaryotic cells, URM1 contributes to oxidative stress tolerance by enhancing ubiquitination of lysine residues in target proteins [7]. URM1 is also implicated

in apoptosis, JNK signaling, and hepatocellular carcinoma (HCC) progression [8]. Elevated URM1 expression in HCC tissues correlates with a poor prognosis. The chronic human T-cell lymphotropic virus type 1 (HTLV-1) oncoprotein, Tax, a novel URM1 target, regulates Tax nuclear/cytoplasmic shuttling. URM1-mediated Tax cytoplasmic relocation upregulates antines and interleukins, which are targets of NF-κB [9]. In HeLa cells, reduced cellular URM1 levels result in significant defects in cell division and multinucleation [9]. URM1 may also be involved in protein sorting regulation, as it resides in small extracellular vesicles [10]. Twenty-one putative URM1 substrates have been identified in humans, including MOCS3 (UBA4 homolog), ATPBD3 (Ncs6 homolog), and CTU2 (Ncs2 homolog), all of which play important roles in oxidative stress response. MOCS3 is a molybdenum cofactor biosynthetic sulfurtransferase [11], whereas ATPBD3 and CTU2 are two thiouracilases required for tRNA sulfurization [7]. These data suggest that URM1 can modify the stress response pathways to exert regulatory effects. Multiple miR-4739 binding sites were present in the 3'-untranslated region of URM1.

This study examined the expression of miRNA-4739 and its regulatory protein URM1 in gastric cancer and adjacent tissues, their role in gastric cancer cell proliferation, migration, and invasion, and the molecular mechanisms underlying gastric cancer regulation.

2. MATERIALS AND METHODS

2.1 Clinical Samples

Fifty gastric cancer tissue samples and their corresponding tumor-adjacent tissues were surgically excised from Yingtan People's Hospital between January 2021 and December 2024. The patients included 11 males and 39 females aged 30 to 68 years, with an average age of (42.0±5.17) years. Histological classification was ulcerative in 18 cases, infiltrative ulcerative in 17 cases, and diffuse infiltrative in 15 cases. The differentiation levels were low, moderate, and high in 20, 16, and 14 cases, respectively. TNM staging was stage I in 12 patients, stage II in 15, stage III in 17, and stage IV in 6. None of the patients had prior chemotherapy or radiotherapy, and their clinical data were comprehensive and without concurrent tumors. All specimens were diagnosed by two professional pathologists, and informed consent was obtained from patients and their families.

This study was approved by the Institutional Ethics Committee of Yingtan People's Hospital (no. 2021-095). All methods were performed in accordance with relevant guidelines and regulations.

2.2 Cell Culture

The human gastric mucosal epithelial cell line, GES-1, and four human gastric cancer cell lines, NCI-N87, AGS, MKN45, and SGC-7901, were used in this study. GES-1 cells are an immortalized normal gastric epithelial cell line. The NCI-N87 cell line derived from human gastric cancer liver metastasis with HER2 positivity was used for the preliminary exploration of the molecular mechanism in the present study. AGS cells are a primary gastric adenocarcinoma cell line with adherent growth characteristics. MKN45 is a highly invasive, semi-adherent gastric cancer cell line derived from liver metastases. SGC-7901 is a classic domestic gastric cancer cell line originating from lymph node metastasis, with stable adherent growth performance and high tumorigenic ability in vivo. Cell lines were purchased from the Shanghai Cell Bank of the Chinese Academy of Sciences. RPMI1640 medium, fetal bovine serum, penicillin, streptomycin, and trypsin were purchased from the American company Gibco (USA).

2.3 Real-time qPCR

Total RNA was extracted from the cells and tissues using TRIzol reagent (Takara, Japan), and its purity and concentration were determined using UV spectrophotometry. The OD260/OD280 ratio was within the range of 1.8 to 2.0. cDNA was synthesized from total RNA using an All-in-One™ miRNA qRT-PCR Detection Kit (GeneCopoeia, NY, USA). The expression levels of miRNA-4739 and URM1 in each sample were detected by real-time fluorescence quantitative PCR using a TaqMan miRNA assay kit (GeneCopoeia, NY, USA). U6 was used as an internal control. The reaction conditions were as follows: 95°C for 10 min and 40 cycles of 95°C for 15 s and 60°C for 60 s. The experiment was repeated thrice, and the relative expression levels of miRNA-4739 and URM1 were calculated using the $2^{-\Delta\Delta Ct}$ method. The specific primer sequences were as follows: miRNA-4739 upstream primer: 5'-GCTGGGACATTGAAAGTCTCA-3', downstream primer: 5'-GATGTTCCCATCGGCGTGTC-3'; URM1 upstream primer: 5'-AAGAAACATCGAGTCACTTTGC-3', downstream primer: 5'-GGTAGTCCAGCTCACCCAGTA-3'; U6 upstream primer: 5'-CTCGCTTCGGCAGCACA-3', and downstream primer: 5'-AACGCTTCAGAATTTGCGT-3'. All sequences were synthesized by Shanghai Sangon Biotechnology Co., Ltd.

2.4 Luciferase reporter system detection

Using the bioinformatics tool TargetScan7, the predicted binding site sequences of miRNA-4739 and the URM1 3'-UTR were designed and synthesized. Wild-type (WT-URM1 3'-UTR) and mutant (MUT-URM1 3'-UTR) plasmids were constructed by Shanghai Sangon Biotechnology Co. Ltd. Logarithmic phase NCI-N87 cells were plated at 1×10^5 cells/well in a 24-well plate and transfected with Lipofectamine 3000, respectively, with miRNA-4739 mimic and its negative control, the WT-URM1 3'-UTR plasmid or MUT-URM1 '-UTR plasmid, for 24 h at 37°C in a fully humidified 5% CO_2 incubator. Cells were washed with PBS, lysed, and luciferase activity was detected according to the double luciferase kit (Beyotime, Shanghai, China) instructions [12].

2.5 Grouping and cell transfection

Logarithmic-phase NCI-N87 cells were plated at a density of 2×10^5 cells/well in 12-well plates. The cells were cultured at 37°C in a fully humidified 5% CO_2 incubator until cell confluence reached over 80%. The cells were divided into five groups: control (blank), miRNA-4739 mimic, miR-NC, miRNA-4739 mimic + pcDNA3-NC, and miRNA-4739 mimic + pcDNA3-URM1. Lipofectamine 3000 (Promega, WI, USA) was used for cell transfection with plasmids at a final concentration of 50 nmol/L in serum-free RPMI1640 medium following the manufacturer's instructions. After incubation for 6 h at 37°C in a fully humidified 5% CO_2 incubator, the medium was replaced with fresh medium and the cells

were further cultured for 48 h for subsequent experiments.

2.6 CCK-8 assay

NCI-N87 cells were incubated for 48 h at 37°C in a fully humidified 5% CO_2 incubator after transfection. Ten microliters of CCK-8 (Tianhang, Hangzhou, China) were added to each well, mixed, and incubated for 2 h at 37°C in a fully humidified 5% CO_2 incubator. The absorbance at 450 nm was measured using an enzyme-linked immunosorbent assay reader, and the experiment was repeated thrice.

2.7 Transwell assay

Diluted Matrigel (50 µl diluted Matrigel) was added to the upper chamber of a 24-well transwell chamber at 37°C for solidification. NCI-N87 cells transfected at a density of 2×10^4 cells/ml were added to the upper chamber (Corning, NY, USA). The lower chamber was filled with 600 µl fresh culture medium containing 10% fetal bovine serum and incubated at 37°C. After 24h of incubation at 37°C and 5% CO_2, the chamber was removed and the culture medium was discarded. The cells at the bottom is then fixed with 4% paraformaldehyde for 30 min, stained with 0.1% crystal violet, washed with PBS to remove excess stain, observed under light microscopy, and images are taken. Five random fields were counted, and the invasion count was calculated using the average value. Matrigel was not used for the migration experiment and the other steps were identical to those used in the invasion assay.

2.8 Western Blot

Cells from each group were collected, washed with PBS, and added to radioimmunoprecipitation assay (RIPA) lysis buffer to extract total proteins. The protein concentrationwas measured using the BCA method. Equivalent amounts of protein samples (50 µg per group) were loaded, and proteins were separated by 10% SDS-PAGE, electroblotted onto PVDF membranes, and blocked overnight at room temperature in 5% skim milk. After blocking, the membranes were rinsed three times with TBST buffer, and then rabbit polyclonal anti-URM1 (ab220490, Abcam, Shanghai, China), rabbit monoclonal anti-JNK1 + JNK2 + JNK3 (phosphoT183+T183+T221) (ab124956, 1:200 Abcam, Shanghai, China), and rabbit monoclonal anti-Caspase-3 antibody (ab32351, 1:200, Abcam, Shanghai, China) primary antibodies were added, and mouse anti-β-actin (1:5000) was used as an internal control. Membranes were then incubated overnight at 4°C. The next day, the primary antibody solution was discarded, the membrane was washed with TBST, the corresponding horseradishperoxidase-labeled secondary antibody solution (1:5000) was added, and the membrane was incubated at room temperature for 1 h. ECL solution (Beyotime, Shanghai, China) was used for staining, and the gel imaging system was used to take pictures. The Image Pro-Plus system was used to analyze the gray value of each protein band and calculate the relative expression level of each protein.

2.9 Construction of PPI Network

URM1 was uploaded to the STRING database (https://string-db.org/). Cytoscape software (version 3.7.1, Seattle, WA, USA) was used to analyze the PPI networks based on the STRING results. The top 10 genes with the highest connectivity were identified as key genes.

2.10 Co-Immunoprecipitation (Co-IP) Assay

Cells were collected 48 h after transfection and washed twice with pre-cooled PBS. Total protein was extracted using radioimmunoprecipitation assay (RIPA) lysis buffer containing 1% protease inhibitor cocktail. The protein concentration was determined using a bicinchoninic acid assay. For each sample, 500 µg of total protein was incubated with 2 µg of rabbit polyclonal anti-URM1 antibody (ab220490; Abcam) or normal rabbit IgG (negative control) overnight at 4°C with gentle rotation. Next, 30 µL of protein A/G agarose beads (Beyotime) were added and incubated for another 4 h at 4°C. The beads were centrifuged at 1,000×g for 5 min at 4°C, and the supernatant was discarded. The beads were washed five times with pre-cooled PBS to remove non-specific binding proteins. Finally, 2× SDS loading buffer was added to the beads, which were boiled at 95°C for 10 min to elute the immune complexes. The eluted proteins were analyzed by western blotting using rabbit monoclonal anti-JNK (Abcam) and anti-URM1 antibodies to detect interactions between URM1 and JNK.

2.11 Protein Disulfide Bond Content Assay

A protein disulfide bond detection kit (Catalog No. ml098837; Mlbio Biotechnology, Shanghai, China) was used for measurement. According to the kit instructions, and the extraction solution was used to extract proteins from 1×10^6 cells per group. Reducing agents were used to break disulfide bonds, and the resulting thiol groups reacted with 5,5'-dithiobis-nitrobenzoic acid (DTNB) to form a yellow compound with a maximum absorption peak at 412 nm. This can be used to calculate the protein disulfide bond content. Reduced glutathione (GSH) were used to generate a standard curve.

2.12 Reactive Oxygen Species (ROS) Detection

Intracellular ROS levels were measured using a DCFH-DA ROS Detection Kit (ml098837; Shanghai, China). Briefly, 48 h after transfection, cells were incubated with 10 µM DCFH-DA probe in serum-free RPMI1640 medium at 37°C for 30 min in the dark. For the inhibitor experiments, cells were pretreated with 20 µM SP600125 (a specific JNK inhibitor) for 2 h before probe incubation. After incubation, the cells were washed thrice with PBS to remove the unbound probe. Fluorescence intensity was detected using a microplate reader at excitation and emission wavelengths of 488 nm and 525 nm, respectively. The ROS levels were calculated relative to those in the control group.

2.13 Statistical Analysis

Data are presented as mean ± standard error. Data analysis was performed using GraphPad Prism10 software with t-test or one-way ANOVA/two-way ANOVA, with $p<0.05$, defined as significant.

3. RESULTS

3.1 miR-4739 is downregulated and URM1 is upregulated in gastric cancer tissue

Quantitative real-time PCR analysis indicated that the expression level of miR-4739 in gastric cancer tissueswas significantly lower than that in adjacent tissues (Figure 1A). According to the gastric cancer TNM staging standard: T1, tumor invades the lamina propria or muscularis mucosae; T2, tumor invadingthe muscularis propria; T3, tumor penetrates the subserosa without visceral peritoneum infiltration; T4, tumor invades serosa (visceral peritoneum) or adjacent or-

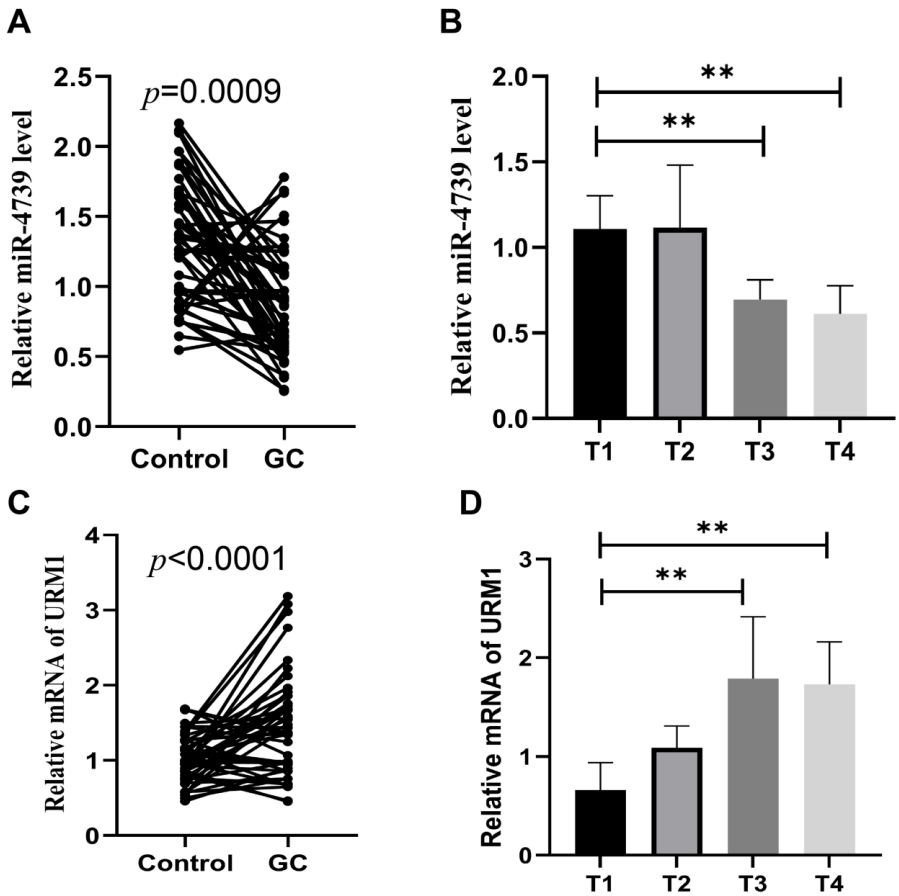

Figure 1 – Downregulation of miR-4739 and upregulation of URM1 in gastric cancer tissues(n=50): A – Real-time qPCR detection of miR-4739 expression in gastric cancer tissues and adjacent tissues; B – Real-time qPCR detection of miR-4739 expression in gastric cancer tissues with different TNM stages; C – Real-time qPCR detection of URM1 expression in gastric cancer tissues and adjacent tissues; D – Real-time qPCR detection of URM1 expression in gastric cancer tissues with different TNM stages.

gans. There was a negative correlation between miR-4739 and TNM staging, and miR-4739 statistical significance was observed in T3 and T4 (Figure 1B). Conversely, the expression level of URM1 mRNA in gastric cancer tissues was significantly higher than that in adjacent tissues (Figure 1C). URM1 exhibited a negative correlation with TNM staging, and statistical significance was observed for T3 and T4 (Figure 1D).

3.2 miR-4739 directly targets URM1

Next, we measured the expression levels of miR-4739 and URM1 in multiple gastric cancer cell lines and normal gastric epithelial GES-1 cells. The results demonstrated that compared to normal GES-1 cells, NCI-N87 and MKN5 cells exhibited significantly lower expression of miR-4739 and markedly higher expression of URM1 (Figure 2A, B). This indicates that NCI-N87 and MKN5 cell lines possess a stronger inhibitory effect on miR-4739 expression and a prominent promoting effect on URM1 expression at the cellular level. Target Scan7 prediction revealed that miR-4739 was complementary to the URM1 3'-UTR (Figure 2C). The dual luciferase reporter assay results showed that the relative fluorescence value of the co-transfected group of miR-4739 mimic and WT-URM1 3'-UTR recombinant plasmid was significantly reduced compared to that of the control group; however, there was no difference in the co-transfected group of miR-4739 mimic and MUT-URM1 3'-UTR recombinant plasmid compared to that of the control group (Figure 2C).

3.3 miR-4739 suppresses tumor growth by targeting URM1

After transfection with miR-4739 mimics, the relative expression level of miR-4739 in the miR-4739 mimic group was significantly higher than that in the control group ($p<0.01$, Figure 3A). The mRNA and protein expression levels of URM1 were significantly lower in the miR-4739 mimic group, indicating that miR-4739 could target and suppress URM1 expression (Figure 3B, C).

At 48h post-transfection, the activity of NCI-N87 cells in the miR-4739 mimic group was significantly lower than that in the control group, and this effect was reversed by URM1 overexpression ($p<0.01$, Figure 3D). Compared to the control group, the number of cells migrating and invading the miR-4739 mimic group was significantly decreased, and this effect was reversed after URM1 overexpression ($p<0.01$, Figure 3E, F).

3.4 URM1 modulates redox reactions and stimulates JNK while inhibiting cell apoptosis.

URM1 was integrated into the STRING database to develop the PPI network. This revealed that URM1 interacts with MOCS3, MPST, CTU1/2, NSF1, ELP3/4, and TRMT-112 (Figure 4A). URM1 functions as a sulfur carrier for the

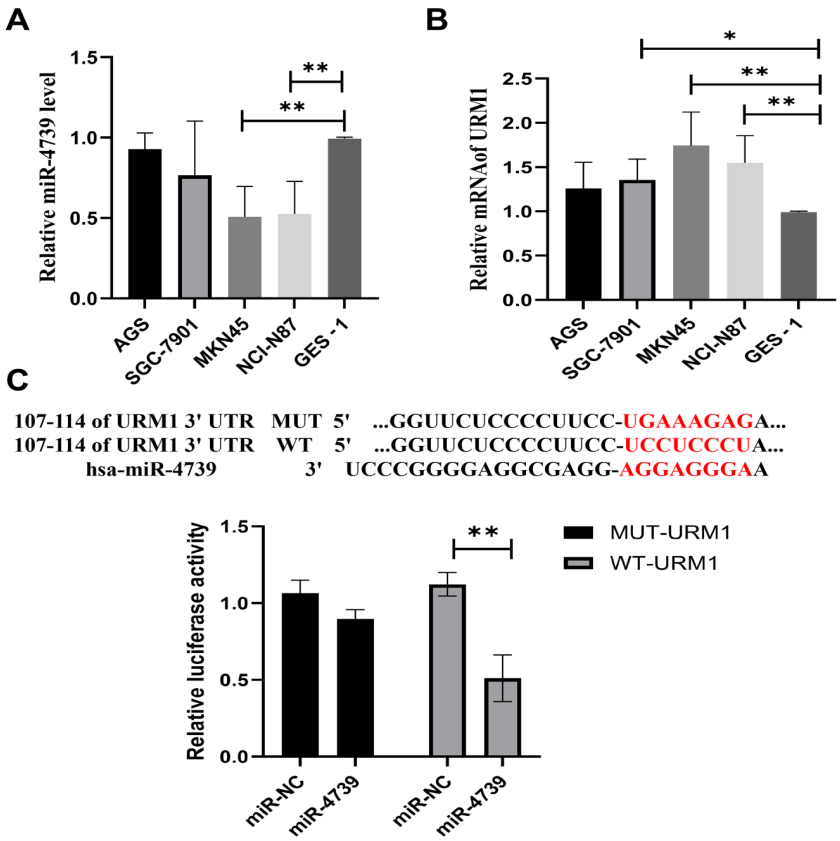

Figure 2 – miR-4739 Directly Targets URM1 in NCI-N87 cells (n=6): A – Real-time qPCR detection of miR-4739 expression inAGS/MKN45/SGC-7901/GES-1cells; B – Real-time qPCR detection of URM1 expression inAGS/MKN45/SGC-7901/GES-1 cells; C – Target Scan 7 prediction the interaction between miR-4739 and the URM1 3'-UTR and Dual luciferase reporter assay.

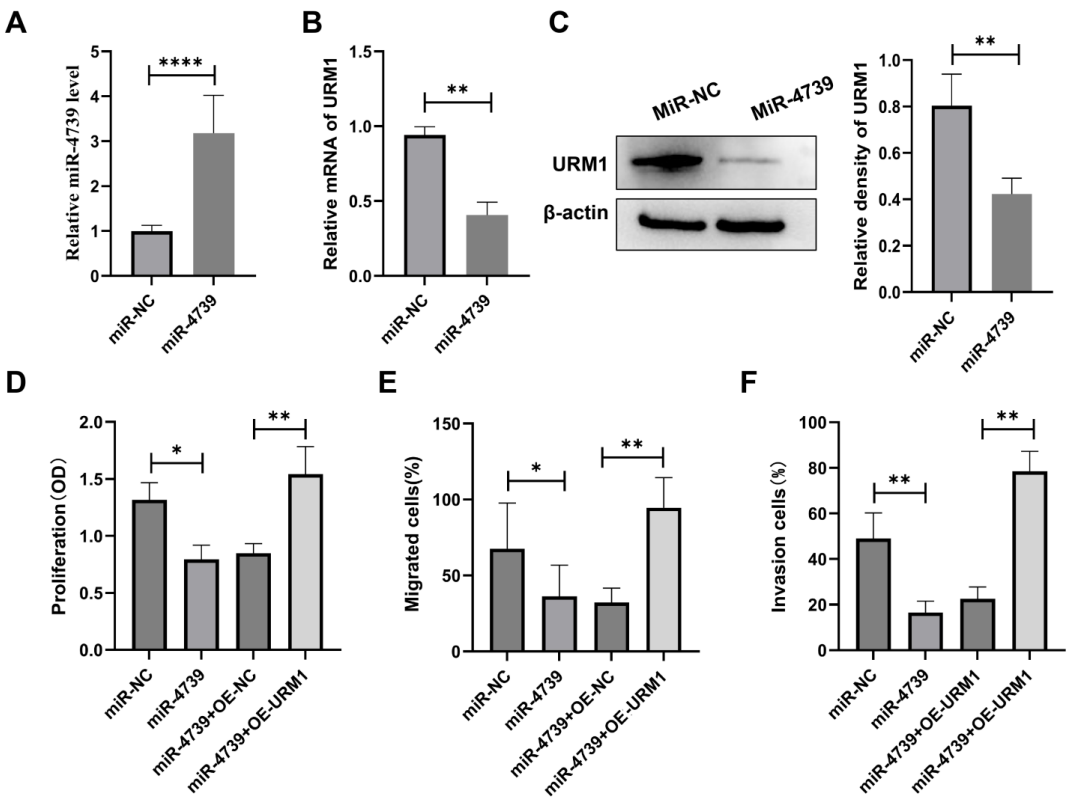

Figure 3 – miR-4739 Suppresses Tumor Growth by Targeting URM1: A – Real-time qPCR detection of miR-4739 (n=6); B – Real-time qPCR detection of URM1 mRNA expression (n=6); C – Western blot detection of URM1 (n=3); D – CCK-8 detection of cell proliferation; E and F – Transwell detection of cell migration and invasion (n=6).

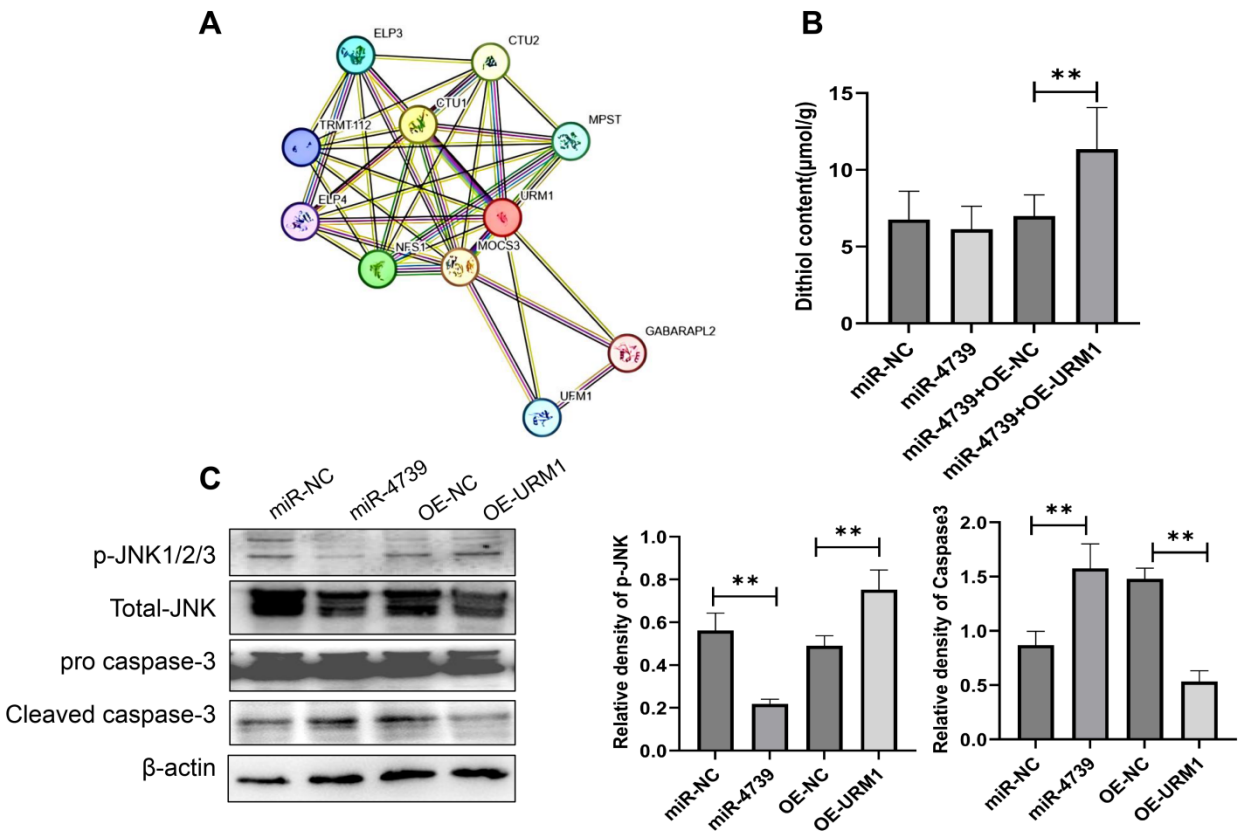

Figure 4 – URM1 protein participates in oxidative stress response: A – Construction of PPI Network using the STRING's online database; B – Protein disulfide bond detection (n=6); C – Western blot analysis of p-JNK, total-JNK, pro caspase-3 and cleaved caspase-3 expression (n=3).

2-thiolation of mcm(5)S(2)U at wobble positions in cytosolic tRNA(Lys), tRNA(Glu), and tRNA(Gln). It serves as a sulfur donor in the tRNA 2-thiolation reaction and is carboxylated (-COSH) at its C-terminus by MOCS3. Sulfur is then transferred to tRNA to form 2-thiolation of mcm(5)S(2)U. Additionally, URM1 functions as a ubiquitin-like protein (UBL) that is covalently linked to lysine residues of target proteins, such as MOCS3, ATPBD3, CTU2, USP15, and CAS. The thiocarboxylated form serves as a substrate for conjugation, and oxidative stress specifically induces the formation of UBL-protein conjugates [13]. Consequently, we further examined protein disulfide bond modifications, which indicated that high URM1 expression significantly promoted disulfide bond formation (Figure 4B). Intracellular oxidative stress regulates JNK and p38 activities through the redox-sensitive complex ASK-1-thioredoxin. Under non-stress conditions, reduced thioredoxin inactive ASK-1. In contrast, oxidized thioredoxin triggers JNK and p38 activation, thereby inhibiting apoptosis [14]. We subsequently analyzed the expression of JNK and the apoptotic protein Caspase-3 via Western blotting, revealing that high URM1 expression enhanced p-JNK1/2/3 expression while suppressing cleavedcaspase-3 expression (Figure 4C).

A co-immunoprecipitation assay was performed to detect the interaction between URM1 and JNK, and the results showed a significant interaction between them (Figure 5A). Furthermore, we used the JNK inhibitor SP60125 (20 μM) to block JNK and observed its effects on oxidative stress. Western blotting showed that the JNK inhibitor SP60125 blocked p-JNK1/2/3 and total JNK expression (Figure 5B). In addition, the JNK inhibitor SP60125 reversed the effect of URM1 in promoting disulfide bond formation and inhibiting ROS production (Figure 5C, D).

5. DISCUSSION

Gastric cancer (GC) remains a leading cause of cancer-related mortality globally, highlighting the urgent need to identify novel regulatory mechanisms and therapeutic targets [1]. miRNAs have emerged as critical regulators of cancer progression, with increasing evidence supporting their role as tumor suppressors or oncogenes [4]. In this study, we systematically explored the role of miRNA-4739 in GC and uncovered a novel regulatory axis involving URM1 and the JNK signaling pathway.

Our clinical data demonstrated that miRNA-4739 was downregulated, whereas URM1 was upregulated in GC tissues, consistent with previous findings that miRNA-4739 acts as a tumor suppressor in prostate cancer [5] and is sequestered by TYMSOS to promote GC progression [6]. Notably, the negative correlation between miRNA-4739 and URM1 expression was strengthened in advanced TNM stages (T3/T4), suggesting their potential as prognostic markers of aggressive GC.

Mechanistically, miRNA-4739 directly targeted the 3'-UTR of URM1, thereby inhibiting URM1 expression. Functional experiments showed that miRNA-4739 overexpression suppressed GC cell proliferation, migration, and invasion, which were rescued by URM1 overexpression, indicating

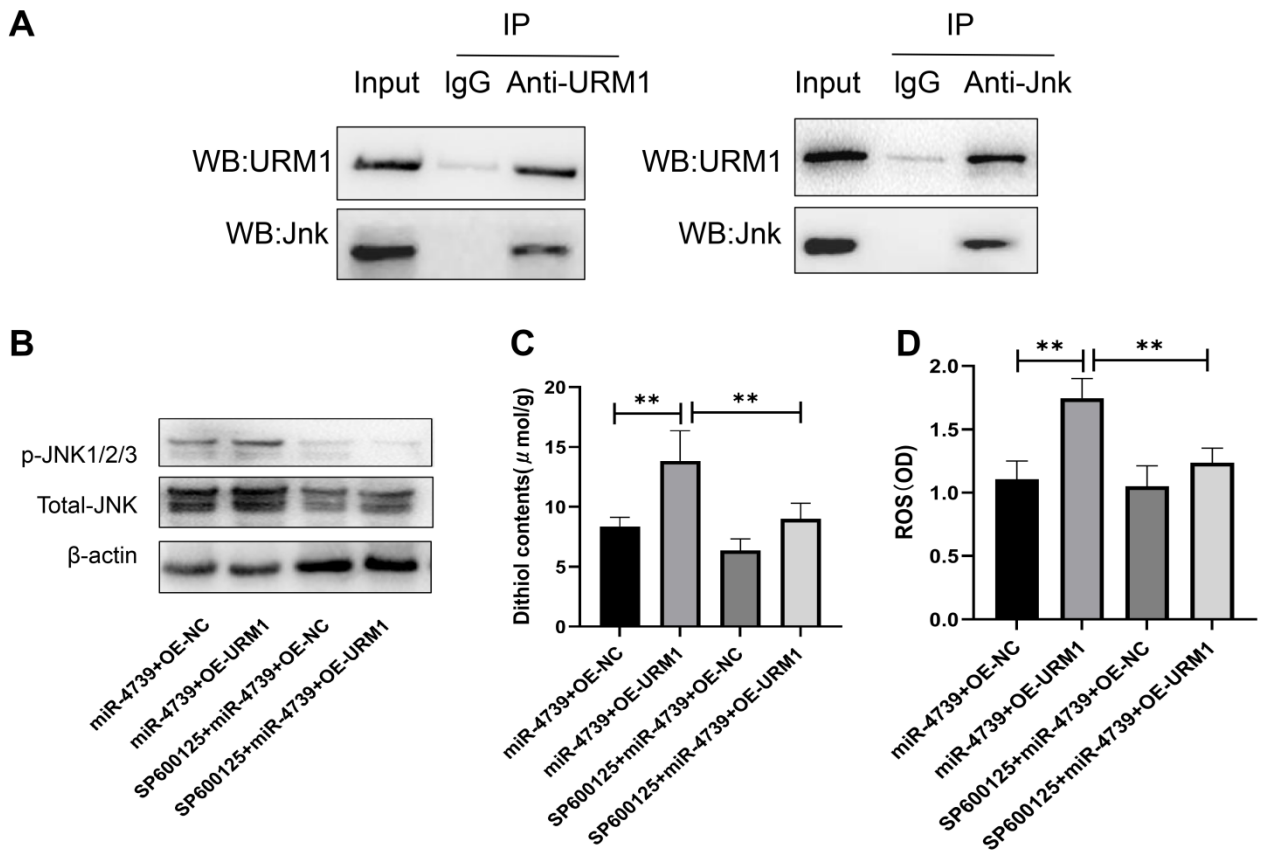

Figure 5 – URM1 interacts with JNK and regulates ROS production via JNK signaling: A – Co-IP assay showing the interaction between URM1 and JNK; B – Western blot analysis of p-JNK and total-JNK expression; C – Protein disulfide bond content assay results (n=6); D – ROS detection results n=6).

that URM1 is a key downstream effector of miRNA-4739. These findings extend previous studies on URM1 as an oncogene in hepatocellular carcinoma [8] and GC, supporting the conserved pro-tumor role of URM1 in digestive system malignancies.

URM1 has been implicated in oxidative stress regulation through tRNA thiolation and ubiquitin-like conjugation [7, 13]. Our results revealed that URM1 promotes protein disulfide bond formation and intracellular ROS production, which are key markers of oxidative stress. Given that redox imbalance can activate survival signaling pathways in tumors [15], we further explored the link between URM1 and JNK, a redox-sensitive kinase involved in apoptosis resistance [14]. Co-IP assays confirmed a direct interaction between URM1 and JNK, and Western blotting showed that URM1 upregulated p-JNK expression, while inhibiting caspase-3, a critical apoptotic executor. Importantly, the JNK inhibitor SP600125 reversed URM1-induced oxidative stress, confirming that URM1 modulates the redox status via JNK activation. These data establish a novel mechanism by which URM1 promotes GC progression: URM1 interacts with JNK to activate JNK signaling, enhance oxidative stress, and suppress apoptosis, thereby facilitating cell proliferation and metastasis.

This study has several strengths. First, the expanded clinical sample size (50 cases) strengthened the reliability of miRNA-4739 and URM1 expression patterns. Second, the integration of Co-IP and ROS detection provides direct evidence of physical and functional interactions between URM1 and JNK. However, since the biological characteristics vary among different gastric cancer cell lines, the regulatory mechanism of the miR-4739/URM1/JNK axis observed in NCI-N87 cells may not be completely consistent with other cell lines such as AGS, MKN45, and SGC-7901. Further validation in multiple gastric cancer cell lines will be conducted in our follow-up research to strengthen the reliability and universality of the present findings, and in vivo animal models are needed to validate the in vitro results. Additionally, the upstream regulators of miRNA-4739 downregulation in GC (e.g., transcriptional factors or competing endogenous RNAs) warrant further investigation.

7. CONCLUSION

Our study identified miRNA-4739 as a tumor suppressor in GC that targets URM1 to inhibit JNK signaling and oxidative stress, thereby suppressing cell proliferation, migration, and invasion and promoting apoptosis. The miRNA-4739/URM1/JNK axis offers new insights into GC pathogenesis and provides potential therapeutic targets for the diagnosis and treatment of GC.

ETHICS APPROVAL AND CONSENT TO PARTICIPATE

The study was approved by the Institutional Ethics Committee of Yingtan People's Hospital (no. 2021-095). All methods were performed in accordance with relevant guidelines and regulations.

AUTHORS' CONTRIBUTIONS

ZZ conceived the study, designed the research, and wrote the manuscript. YZ collected data and conducted the study. YX analyzed the data. All authors have read and approved the submitted version.

ACKNOWLEDGEMENTS

Not applicable.

FUNDING

Not applicable.

CONFLICT OF INTEREST

The authors declare no competing interest.

REFERENCES

1. Smyth, E.C., Nilsson, M., Grabsch, H.I., van Grieken, N.C., Lordick, F. Gastric cancer // Lancet. – 2020. – Vol. 396(10251). – P. 635–648. https://doi.org/10.1016/S0140-6736(20)31288-5

2. Eusebi, L.H., Telese, A., Marasco, G., Bazzoli, F., Zagari, R.M. Gastric cancer prevention strategies: A global perspective // Journal of Gastroenterology and Hepatology. – 2020. – Vol. 35(9). – P. 1495–1502. https://doi.org/10.1111/jgh.15037

3. Harada, K., Sakamoto, N., Ukai, S., Yamamoto, Y., Pham, Q.T., Taniyama, D., Honma, R., Maruyama, R., Takashima, T., Ota, H., Takemoto, Y., Tanabe, K., Ohdan, H., Yasui, W. Establishment of oxaliplatin-resistant gastric cancer organoids: Importance of myoferlin in the acquisition of oxaliplatin resistance // Gastric Cancer. – 2021. – Vol. 24(6). – P. 1264–1277. https://doi.org/10.1007/s10120-021-01206-4

4. Zhang, Y., Han, T., Feng, D., Li, J., Wu, M., Peng, X., Wang, B., Zhan, X., Fu, P. Screening of non-invasive miRNA biomarker candidates for metastasis of gastric cancer by small RNA sequencing of plasma exosomes // Carcinogenesis. – 2020. – Vol. 41(5). – P. 582–590. https://doi.org/10.1093/carcin/bgz186

5. Wang, X., Chen, Q., Wang, X., Li, W., Yu, G., Zhu, Z., Zhang, W. ZEB1 activated-VPS9D1-AS1 promotes the tumorigenesis and progression of prostate cancer by sponging miR-4739 to upregulate MEF2D // Biomedicine & Pharmacotherapy. – 2020. – Vol. 122. – Article 109557. https://doi.org/10.1016/j.biopha.2019.109557

6. Gu, Y., Wan, C., Zhou, G., Zhu, J., Shi, Z., Zhuang, Z. TYMSOS drives the proliferation, migration, and invasion of gastric cancer cells by regulating ZNF703 via sponging miR-4739 // Cell Biology International. – 2021. – Vol. 45(8). – P. 1710–1719. https://doi.org/10.1002/cbin.11610

7. Van der Veen, A.G., Schorpp, K., Schlieker, C., Buti, L., Damon, J.R., Spooner, E., Ploegh, H.L., Jentsch, S. Role of the ubiquitin-like protein Urm1 as a noncanonical lysine-directed protein modifier // Proceedings of the National Academy of Sciences of the United States of America. – 2011. – Vol. 108(5). – P. 1763–1770. https://doi.org/10.1073/pnas.1014402108

8. Cheng, X., Zhang, Y., Song, F., Song, F., Gao, C., Liang, X., Wang, F., Chen, Z. URM1 promoted tumor growth and suppressed apoptosis via the JNK signaling pathway in hepatocellular carcinoma // OncoTargets and Therapy. – 2020. – Vol. 13. – P. 8011–8025. https://doi.org/10.2147/OTT.S258843

9. Hleihel, R., Khoshnood, B., Dacklin, I., Omran, H., Mouawad, C., Dassouki, Z., El-Sabban, M., Shirinian, M., Grabbe, C., Bazarbachi, A. The HTLV-1 oncoprotein Tax is modified by the ubiquitin-related modifier 1 (Urm1) // Retrovirology. – 2018. – Vol. 15(1). – Article 33. https://doi.org/10.1186/s12977-018-0415-4

10. Abramowicz, A., Wojakowska, A., Marczak, L., Lysek-Gladysinska, M., Smolarz, M., Story, M.D., Polanska, J., Widlak, P., Pietrowska, M. Ionizing radiation affects the composition of the proteome of extracellular vesicles released by head-and-neck cancer cells in vitro // Journal of Radiation Research. – 2019. – Vol. 60(3). – P. 289–297. https://doi.org/10.1093/jrr/rrz001

11. Chowdhury, M.M., Dosche, C., Löhmannsröben, H.G., Leimkühler, S. Dual role of the molybdenum cofactor biosynthesis protein MOCS3 in tRNA thiolation and molybdenum cofactor biosynthesis in humans // Journal of Biological Chemistry. – 2012. – Vol. 287(21). – P. 17297–17307. https://doi.org/10.1074/jbc.M112.351429

12. Liu, D., Tang, Z., Bajinka, O., Dai, P., Wu, G., Qin, L., Tan, Y. miR-34b/c-5p/CXCL10 axis induced by RSV infection mediates a mechanism of airway hyperresponsive diseases // Biology. – 2023. – Vol. 12(2). – Article 317. https://doi.org/10.3390/biology12020317

13. Pabis, M., Termathe, M., Ravichandran, K.E., Kienast, S.D., Krutyhołowa, R., Sokołowski, M., Jankowska, U., Grudnik, P., Leidel, S.A., Glatt, S. Molecular basis for the bifunctional Uba4-Urm1 sulfur-relay system in tRNA thiolation and ubiquitin-like conjugation // EMBO Journal. – 2020. – Vol. 39(19). – Article e105087. https://doi.org/10.15252/embj.2020105087

14. Nagai, H., Noguchi, T., Takeda, K., Ichijo, H. Pathophysiological roles of ASK1-MAP kinase signaling pathways // Journal of Biochemistry and Molecular Biology. – 2007. – Vol. 40(1). – P. 1–6. https://doi.org/10.5483/BMBRep.2007.40.1.001

15. Matsuzawa, A. Thioredoxin and redox signaling: Role of the thioredoxin system in control of cell fate // Archives of Biochemistry and Biophysics. – 2017. – Vol. 617. – P. 101–105. https://doi.org/10.1016/j.abb.2016.09.011